Sensors and Materials, Vol. 37, No. 2 (2025) 463–473
MYU Tokyo

S & M 3921

Basic Study of 3 mm Dose Equivalent Measurement Technique Using the Stacked Thermoluminescent Dosimeter Method

Hinata Fujiwara, Toru Negishi, Leo Takahashi, and Kiyomitsu Shinsho*

Tokyo Metropolitan University, 7-2-10 Higashi-Ogu, Arakawa-ku, Tokyo 116-8551, Japan

(Received November 11, 2024; accepted December 25, 2024)

Keywords: 3 mm dose equivalents, stacked thermoluminescent dosimeter method, eye lens, effective energy, incident photons

Japan revised the dose limit for the lens of the eye in 2021 to 20 mSv/year on a five-year average, with a maximum of 50 mSv/year in any one year. This represents a significant reduction from the previous limit of 150 mSv/year and necessitates accurate measurements of the 3 mm dose equivalent. Current dosimeters, such as DOSIRIS, EYE-D™, and Vision Badge, lack the ability to provide incident photon energy information, which potentially leads to the overestimation of the actual dose to the eye lens, especially in low-energy photon environments. In this study, we investigate a method of estimating the incident photon energy using a novel stacked thermoluminescent dosimeter (TLD) arrangement. BeO and Al_2O_3 phosphors were stacked and the absorbed dose ratios were measured to estimate the effective energy of incident photons. The results showed that the stacked TLD method can accurately estimate photon energies in the range of 26–87 keV, which makes this a promising approach to improve dosimetry accuracy for healthcare workers exposed to ionizing radiation. The detection limits for BeO and Al_2O_3 were also determined to be 2.49 and 3.35 μGy, respectively. This technique has potential as a new method for lens dosimetry to provide more accurate exposure assessments for occupational radiation safety.

1. Introduction

The dose limit for the lens of the eye was changed in 2021 to 20 mSv/year on a five-year average and not exceeding 50 mSv/year in any one year, which is less than one-seventh of the previous limit of 150 mSv/year. It has also been recommended to measure 3 mm dose equivalents from 1 cm or 70 μm dose equivalents, whichever is appropriate for the measurement of the equivalent dose in the lens of the eye. The 3 mm dose equivalent is calculated by multiplying the measured air kerma by a 3 mm dose equivalent conversion factor determined by calculation. The 3 mm dose equivalent conversion coefficient is highly dependent on the incident photon energy; therefore, information on the photon energy incident on the lens of the eye is necessary to correctly measure the 3 mm dose equivalent. However, current dosimeters that support 3 mm dose equivalents, such as Chiyoda Technol DOSIRIS,[(1)] RADCARD EYE-D™,[(2)] and Nagase

*Corresponding author: e-mail: shinsho@tmu.ac.jp
https://doi.org/10.18494/SAM5475

ISSN 0914-4935

Landauer Vision Badge,[3] are not capable of obtaining information on the incident photon energy. For this reason, the 3 mm dose equivalent conversion coefficient is large for safety reasons. The 3 mm dose equivalent conversion coefficient changes significantly in the low-energy region down to approximately 100 keV, with a maximum difference of 14 times. Therefore, it is possible that the current dosimetry overestimates the equivalent dose in the lens compared with the actual equivalent dose in the lens of the eye. In 2016, the Council of Personal Dosimetry Organizations reported that approximately 2400 healthcare workers engaged in interventional radiology (IVR) and other activities in Japan and exceeded the dose limit of 20 mSv/year.[4] Current safety-oriented technologies create problems, such as the fear that some medical staff members may unnecessarily exceed dose limits and the difficulty in obtaining basic data essential for a correct cataract risk discussion. Before the dose limits were lowered, the dose limit for the lens of the eye (150 mSv) was higher than those for other organs, so that the dose to the lens was not measured separately.[5] Therefore, until the early 1990s, only a few studies were focused on lens radiation exposure control. However, the International Commission on Radiological Protection 2000 reported a high risk of lens damage in healthcare workers engaged in IVR, which led to active research regarding lens dosimetry. In 2008, a method was reported in which a dosimeter measuring 1 cm or 70 μm dose equivalent, which was typically worn on the torso, was worn at neck level, and the dose to the lens was evaluated from the measured values by correction. However, this evaluation method overestimated the dose to the lens by approximately 25%.[6] In a subsequent 2011 project by the Optimization of Radiation Protection for Medical Staff, a new cylindrical phantom that approximated the human head was proposed, and the conversion coefficients from air kerma to 3 mm dose equivalent for incident photons were determined.[7,8] As a result of research led by the manufacturer Radcard, an LiF:Mg, Cu, P (trade name MCP-N detector) covered by a polyamide capsule dedicated to the measurement of 3 mm dose equivalent was successfully developed.[2] This is a new type of dosimeter where the detector can be fixed close to the eye. Around the same time, research was also conducted to determine the optimal location for the detector on the wearer, which was concluded to be near the left eye.[2,9,10] Further research was also conducted to optimize the mounting method, location, and detector type.[11–13] Dosimeters that can be worn inside protective eyewear have also been developed in recent years.[1,14] However, none of these reports proposed a dosimeter that can obtain a 3 mm dose equivalent based on incident photon energy information.[15]

Therefore, we have focused our research on the development of a dosimeter that can acquire information on the photon energy incident on the lens. Takagi *et al.* previously proposed a method of calculating the incident photon energy by stacking three thermoluminescent (TL) phosphors in a Monte Carlo simulation.[16] The method consists of stacking 1-mm-thick plates of TL phosphors in the order of BeO, Al_2O_3, and BeO from the source side and calculating the incident photon energy from the absorbed dose ratio of each. The type and stacking order of the TL phosphors are the results of a Monte Carlo simulation study of the optimal combination of three plates of TL phosphors with large differences in absorbed dose ratio. Here, we have investigated a method of calculating the effective energy of incident photons using actual TL phosphors, based on the proposal by Takagi *et al.*[16] using Monte Carlo simulations.

2. Materials and Methods

2.1 BeO ceramic plates

The BeO ceramic plates (Thermalox 995, Materion) employed in this work are elements with a BeO content of 99.5% or higher (Fig. 1). The other constituents in the plates are Si, Mg, Na, Al, Fe, Ca, and Zn, and their contents are given in Table 1. The size of the BeO plates was $(10 \pm 1) \times (10 \pm 1) \times 0.7$ mm^3 with a density of 2.85 g/cm^3 and an effective atomic number of 7.13.[17]

2.2 Al_2O_3:Cr ceramic plates

Plates with more than 99.5% Al_2O_3 and 0.05% Cr_2O_3 (Al_2O_3:Cr; Chiba Ceramic MFG. Co, Ltd.) were also used (Fig. 2). The other constituents in the plates are SiO_2, Fe_2O_3, Na_2O, Cr, Cd, Pb, and Hg, and their contents are given in Table 2.[18–20] The size of the Al_2O_3:Cr plates was $(10 \pm 1) \times (10 \pm 1) \times 0.7$ mm^3 with a density of 3.7 g/cm^3 and an effective atomic number of 11.13.[20]

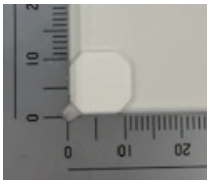

Fig. 1. (Color online) Photograph of BeO ceramic plate (unit: mm).

Table 1
Chemical composition of BeO ceramic plates.

Element	Si	Mg	Na	Al	Fe	Ca	Zn
Content (wt%)	0.1800	0.0922	0.0173	0.0046	0.0032	0.0031	0.0020

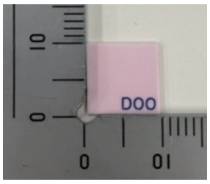

Fig. 2. (Color online) Photograph of Al_2O_3:Cr ceramic plate (unit: mm).

Table 2
Chemical composition of Al_2O_3:Cr ceramic plates.

Element	SiO_2	Fe_2O_3	Na_2O	Cr	Cd	Pb	Hg
Content (wt%)	0.1000	0.0500	0.1000	0.0002	0.0001	0.0001	0.0001

2.3 Effective energy estimation method using stacked thermoluminescent dosimeter (TLD)

2.3.1 Calculation of effective energy using an ionization chamber

The effective energy was calculated from the relationship between the Cu half-value layer (HVL) and the linear attenuation coefficient after the actual measurement of the Cu HVL using an ionization chamber. An industrial X-ray irradiation system (Seifert ISOVOLT Titan neo HP, Waygate Technologies) was used. The ionization chamber was a 1 L spherical ionization chamber (32002, EMF Japan) with an electrometer (EMF520R, EMF Japan). The additional filter was a Pb plate. Al and Cu HVLs were measured using Al and Cu with a purity of 99.9% or higher. The tube voltages, filters, and effective energies used in this study are listed in Table 3.

The following relationship is established between the HVL T and the linear attenuation coefficient μ, which was calculated from the measured HVL using Eq. (1), and the mass attenuation coefficient μ/ρ was obtained by dividing by the density.

$$\mu = \ln 2/T \tag{1}$$

The effective energy was calculated from the relationship between the mass attenuation coefficient of Cu and the effective energy[21] (Fig. 3).

2.3.2 Measurement of half-valued layer and estimation of effective energy using stacked TLDs

Process 1: HVL measurement with stacked TLDs

The X-ray irradiation device and irradiation conditions were the same as those used for the ionization chamber measurement. The irradiation system is shown in Fig. 4. The TL phosphors were stacked as BeO_1, Al_2O_3, and BeO_3 from the vacuum tube side (Fig. 5) and covered with light-shielding vinyl.

Process 2: TL glow curve measurements

Irradiated TL phosphors were stored in a refrigerator at 1–2 °C for 1 day to reduce fading effects. TL glow curves were measured using an in-house developed measurement instrument

Table 3
Tube voltages, filters, and effective energies used in this study.

X-ray tube voltage (kV)	Filter (mm)	Effective energy (keV)
40	without	26
80	without	36
110	without	40
80	Pb 0.2	55
80	Pb 2	77
150	Pb 2	87

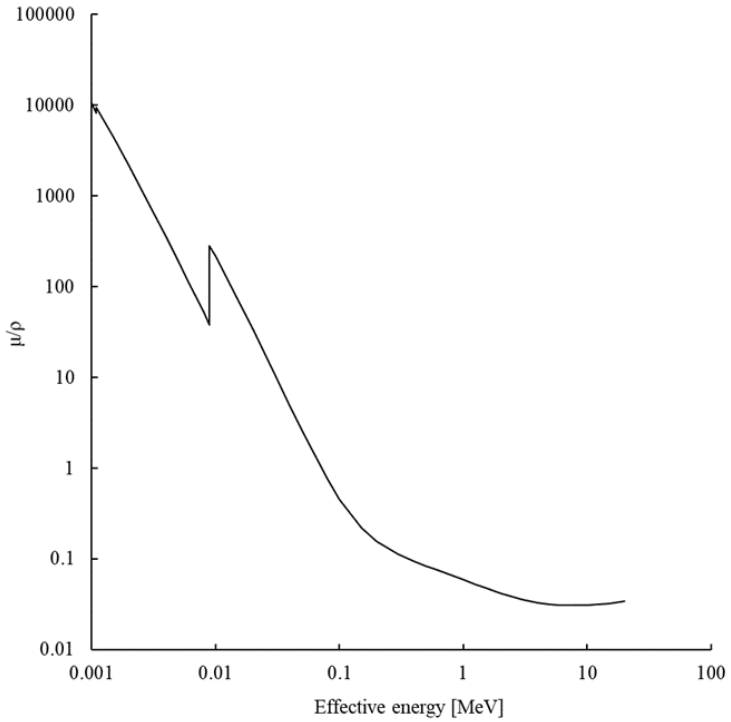

Fig. 3. Relationship between mass attenuation coefficient and effective energy.[21]

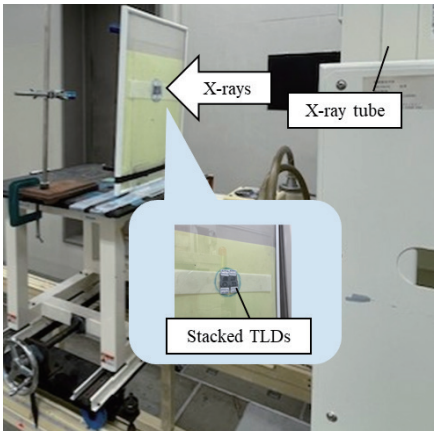

Fig. 4. (Color online) Photograph of the irradiation system.

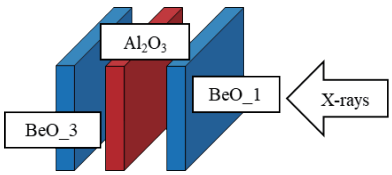

Fig. 5. (Color online) Schematic illustration of the stacked TLD.

(Fig. 6) that consisted of a dark box, a programmable temperature controller (SCR-SHQ-A, Sakaguchi Electric Heaters Co., Ltd.), and a PC. A heater, a photon-counting head (H11890-210, Hamamatsu Photonics), and a focusing lens were installed inside the dark box. The sample chamber above the heater was sealed with a quartz glass lid, and the TL intensity was recorded from 50 to 400 °C. TL was focused by a condenser lens and detected by a photon counting head.

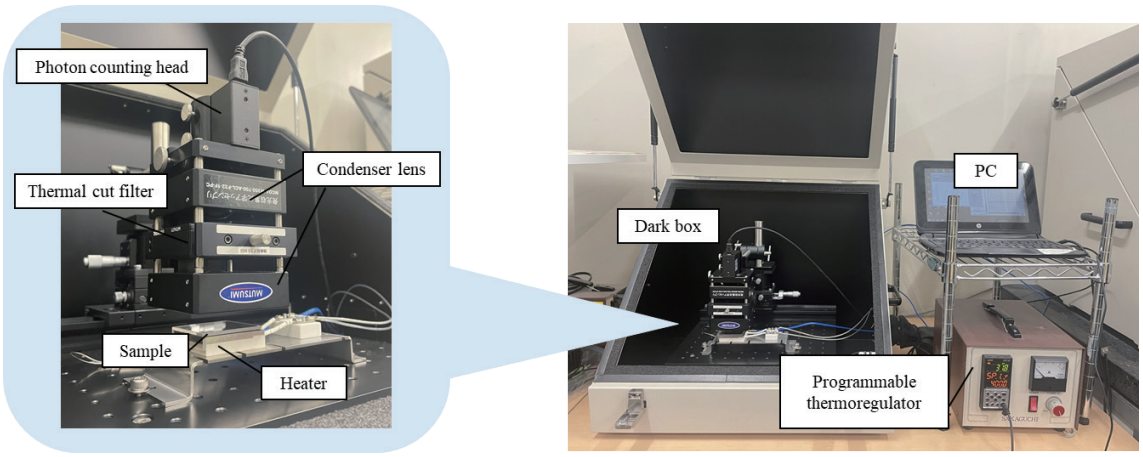

Fig. 6. (Color online) Glow curve measurement instrument.

The TL amount and the temperature of the heater at this time were recorded on the PC. Figure 7 shows the layout of the TL device.

Process 3: Dose conversion tables for TL and calculation of the absorbed dose ratios.

Dose conversion tables were prepared for BeO and Al_2O_3 at an effective energy of 77 keV using a Pb plate as an additional filter. Absorbed doses were measured using a spherical ionization chamber (TN32002, EMF Japan) and an electrometer (EMF520R, EMF Japan). Absorbed dose ratios were calculated using the prepared dose conversion tables.

Process 4: Calculation of effective energy from the measured absorbed dose ratio of stacked TLDs

The effective energy was obtained from the measured absorbed dose ratios by using the relationship between absorbed dose ratio and effective energy (Fig. 8) reported by Takagi *et al.*[16] In the energy region below 40 keV, the ratio of BeO_1 to BeO_3, which has a large absorbed dose ratio, was used, and in the energy region from 40 to 120 keV, the ratio of Al_2O_3:Cr to BeO_3 was used in the energy range from 40 to 120 keV.

3. Results and Discussion

3.1 Dose conversion tables for TL and calculation of detection dose limits

The TL intensity-to-dose conversion tables for BeO and Al_2O_3:Cr measured according to Process 3 are shown in Figs. 9 and 10. The TL intensity was estimated by integrating over a range of ±77 degrees from the peak temperature. Although an infrared cut filter was used during the measurement, no spectroscopic analysis was performed.

The TL intensity for BeO increased quadratically with the dose (Fig. 9). The relationship between the dose and TL intensity can be expressed by the following equation from the approximation formula:

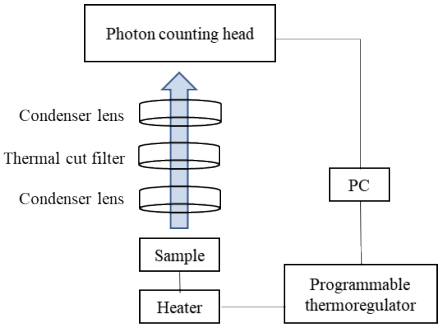

Fig. 7. (Color online) Schematic diagram of the glow curve measurement instrument.

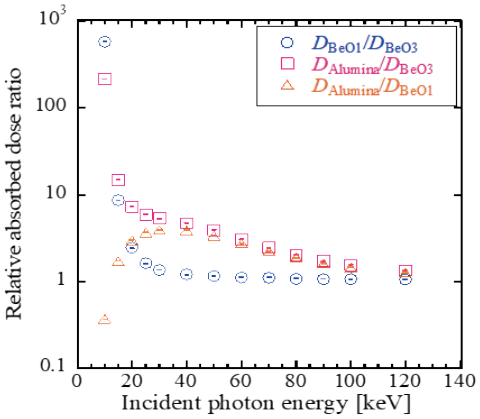

Fig. 8. (Color online) Results from Monte Carlo simulations.[17]

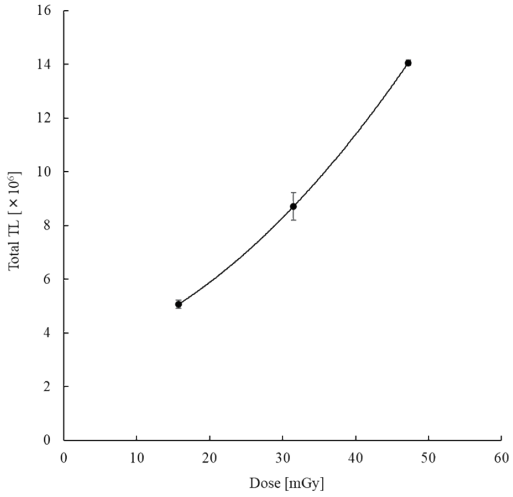

Fig. 9. TL dose response curve of BeO.

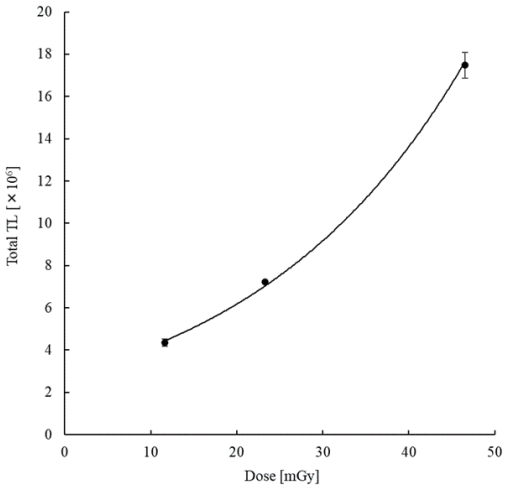

Fig. 10. TL dose response curve of Al_2O_3:Cr.

$$Total\ TL = (3.5 \times 10^3)\ Dose^2 + (6.8 \times 10^4)\ Dose + 3.0 \times 10^6. \quad (2)$$

The absorbed doses of BeO_1 and BeO_3 by the laminated TLDs were calculated using this equation. The dose at the estimated limit of BeO calculated from 3σ of the background was 2.49 μGy.

The TL intensity of Al_2O_3:Cr increased quadratically with the dose (Fig. 10) as in the TL response curve of BeO. The relationship between the dose and TL intensity can be expressed by the following equation from the approximate formula:

$$Total\ TL = (5.5 \times 10^3)\ Dose^2 + (5.4 \times 10^4)\ Dose + 3.0 \times 10^6. \quad (3)$$

The absorbed doses for Al_2O_3:Cr by the laminated TLDs were calculated using this equation. The dose at the estimated limit of Al_2O_3:Cr calculated from 3σ of the background was 3.35 μGy.

3.2 HVL measurement with stacked TLDs

Table 4 shows the absorbed doses of the stacked TLDs when irradiated under the conditions shown in Table 3. The irradiation time differs with the effective energy based on the recommended use of the device. The effective energy in Table 4 and the absorbed dose ratio for each layer of the stacked TLDs are shown in Fig. 11.

Figure 11 shows the absorbed dose ratios of BeO_1/BeO_3, Al_2O_3:Cr/BeO_1, and Al_2O_3:Cr/BeO_3, which all decreased with increasing effective energy. In addition, the absorbed dose ratio of BeO_1/BeO_3 has a smaller change with respect to the effective energy than that of

Table 4
Relationship between effective energy measured by the ionization chamber and absorbed dose of the stacked TLDs.

	Dose of Stacked TLDs (mGy)		
Effective energy (keV) (ion chamber)	BeO_1	Al_2O_3:Cr	BeO_3
26	49.0	—	37.4
36	131	521	108
40	188	708	160
55	27.4	82.8	26.5
77	11.7	23.8	11.3
87	31.9	38.7	28.4

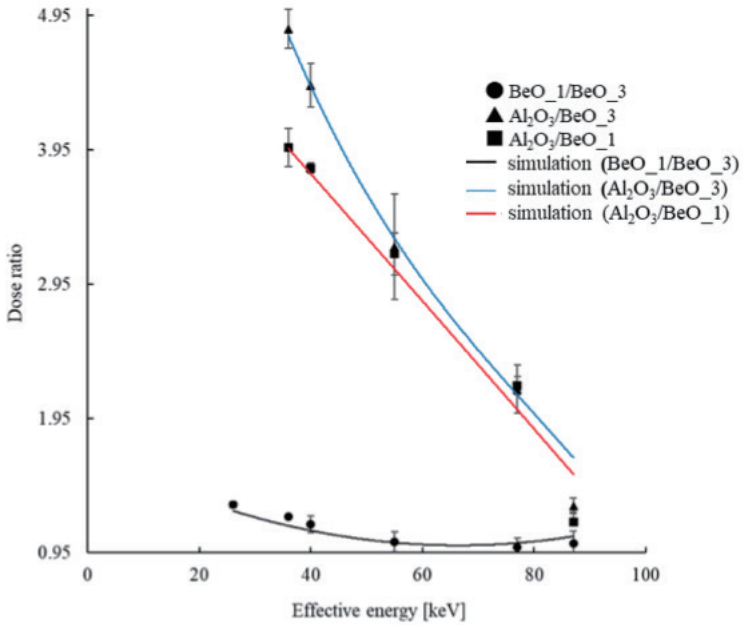

Fig. 11. (Color online) Relationship between effective energy and absorbed dose ratio by stacked TLDs (the simulation results are based on the report of Takagi *et al.*[16]).

Al_2O_3:Cr/BeO_1 or Al_2O_3:Cr/BeO_3. When the effective energy is above 55 keV, the absorbed doses of BeO_1 on the source side and BeO_3 located away from the source are almost the same, and the absorbed dose ratio is constant up to 87 keV. This is considered to be due to the disappearance of the difference between the absorbed doses of BeO_1 and BeO_3 because of the higher transmission of incident photons as the effective energy increases. On the other hand, the absorbed dose ratios for Al_2O_3:Cr/BeO_1 and Al_2O_3:Cr/BeO_3 showed similar trends and decreased with increasing effective energy, provided that the absorbed dose ratio for Al_2O_3:Cr/BeO_3 was larger than that for Al_2O_3:Cr/BeO_1 when the effective energy was below 40 keV. This may be due to fewer photons reaching BeO_3 than BeO_1 with a lower effective energy. These results were almost the same as those reported by Takagi *et al.*[16]

3.3 Calculation of effective energy by stacked TLDs

On the basis of the relationship between the effective energy and the absorbed dose ratio for the stacked TLDs reported by Takagi *et al.*,[16] the effective energy was calculated from the absorbed dose ratio obtained from the stacked TLDs (Fig. 11, Tables 5–7). The tables show the effective energy calculated from the half-valued layer values measured with the ionization chamber, the absorbed dose ratio of the measured stacked TLDs (this study), the absorbed dose ratio of the stacked TLDs calculated by Monte Carlo simulation,[16] and the absorbed dose ratio of the measured stacked TLDs calculated by Process 4 using the effective energy (this study).

The effective energies derived from the BeO_1/BeO_3 absorbed dose ratios for laminated TLDs were similar to those obtained from the ionization chamber in the range of 26–40 keV, although there was some variation. This variation is considered to be due to the small change in absorbed dose ratio with respect to the increase in effective energy in this region, so that small differences in absorbed dose ratio have a large effect on the resultant effective energy. The effective energy could not be calculated because the absorbed dose ratio for the stacked TLDs takes a constant value when the effective energy is above 55 keV. The results were similar to those reported by Takagi *et al.*[16] Tables 6 and 7 show that the effective energies derived from the absorbed dose ratios for Al_2O_3:Cr/BeO_3 and Al_2O_3:Cr/BeO_1 for the stacked TLDs are comparable to the effective energy results obtained from the ionization chamber in the range of 26–40 keV. Compared with the change in absorbed dose ratio for the effective energy of BeO_1/BeO_3, the changes in absorbed dose ratio for Al_2O_3:Cr/BeO_3 and Al_2O_3:Cr/BeO_1 were

Table 5
Estimation of effective energy for BeO_1/BeO_3.

Effective energy (ion chamber) (keV)	Dose ratio (this study)	Dose ratio (Takagi *et al.*[16])	Effective energy (this study) (keV)
26	1.31	1.30	24
36	1.22	1.10	31
40	1.16	1.10	44
55	1.03	1.05	—
77	0.99	1.05	—
87	1.02	1.05	—

Table 6
Estimation of effective energy for Al_2O_3:Cr /BeO_3.

Effective energy (ion chamber) (keV)	Dose ratio (this study)	Dose ratio (Takagi *et al.*[16])	Effective energy (this study) (keV)
36	4.85	4.75	34.0
40	4.41	4.50	40.4
55	3.23	3.25	58.5
77	2.17	2.15	74.5
87	1.30	1.65	87.7

Table 7
Estimation of effective energy for Al_2O_3:Cr /BeO_1.

Effective energy (ion chamber) (keV)	Dose ratio (this study)	Dose ratio (Takagi *et al.*[16])	Effective energy (this study) (keV)
36	3.97	3.90	35.8
40	3.81	3.85	39.1
55	3.18	3.05	52.6
77	2.20	2.00	73.1
87	1.18	1.55	94.6

larger (Fig. 11), which indicates that the Al_2O_3:Cr/BeO_3 or Al_2O_3:Cr/BeO_1 results can be used to estimate the effective energy for the X-ray energy range used in X-ray diagnostics. It is preferable to use Al_2O_3:Cr/BeO_3, which has a higher absorbed dose ratio, than Al_2O_3:Cr/BeO_1 for measurements in the region below 40 keV. It is concluded that the use of BeO_3 is preferable for the same reason given in the report by Takagi *et al.*[16] However, in the energy region below 20 keV, which was not considered in this study, the combination of BeO_1/BeO_3 with Al_2O_3:Cr /BeO_3 and Al_2O_3:Cr /BeO_1 may be available, based on the results in Fig. 8 reported by Takagi *et al.*[16]

4. Conclusion

A basic study on a method of estimating the incident photon energy with stacked TL phosphors was conducted. The effective energy estimation method using the absorbed dose ratio of TLDs stacked in the order of BeO, Al_2O_3:Cr, and BeO from the source side was determined to be useful. The Al_2O_3:Cr/BeO_3 or Al_2O_3:Cr/BeO_1 absorbed dose ratios for stacked TLDs are recommended for the estimation of the effective energy in the range of 26–87 keV. In the energy region below 20 keV, not only Al_2O_3:Cr/BeO_3 and Al_2O_3:Cr/BeO_1 but also BeO_1/BeO_3 combinations may be used. The detection limits for BeO and Al_2O_3:Cr were 2.49 and 3.35 μGy, respectively. This method has shown potential as a new lens dosimeter that can estimate photon energy incident on the lens of the eye. In the future, we will investigate the effectiveness of this method in the case of broader energy spectra and its directional dependence to advance its practical application.

References

1 H. Ishii, Y. Haga, M. Sota, Y. Inaba, and K. Chida: J. Radiol. Prot. **39** (2019) N19. https://doi.org/10.1088/1361-6498/ab2729
2 P. Bilski, J.-M. Bordy, J. Daures, M. Denoziere, E. Fantuzzi, P. Ferrari, G. Gualdrini, M. Kopeć, F. Mariotti, F. Monteventi, and S. Wach: Radiat. Meas. **46** (2011) 1239. https://doi.org/10.1016/j.radmeas.2011.04.031
3 T. Arai, K. Ono, K. Wakamatsu, I. Yamaguchi, and N. Kunugita: Jpn. Assoc. Radiol. Technol. **69** (2022) 393. https://www.jart.jp/docs/2022-04_paper5.pdf
4 S. Yokoyama, S. Suzuki, H. Toyama, S. Arakawa, S. Inoue, Y. Kinomura, and I. Kobayashi: Radiat. Prot. Dosim. **173** (2017) 218. https://doi.org/10.1093/rpd/ncw321
5 C. Eleftheria, F. Paolo, C. B. Olivera, G. Merce, S. M. Marta, and O. Una: J. Radiol. Prot. **35** (2015) R17. https://doi.org/10.1088/0952-4746/35/3/R17
6 P. Clerinx, N. Buls, H. Bosmans, and J. de Mey: Radiat. Prot. Dosim. **129** (2008) 321. https://doi.org/10.1093/rpd/ncn148
7 G. Gualdrini, F. Mariotti, S. Wach, P. Bilski, M. Denoziere, J. Daures, J.-M. Bordy, P. Ferrari, F. Monteventi, and E. Fantuzzi: Radiat. Prot. Dosim. **144** (2011) 473. https://doi.org/10.1093/rpd/ncr011
8 J. M. Bordy, G. Gualdrini, J. Daures, and F. Mariotti: Radiat. Prot. Dosim. **144** (2011) 257. https://doi.org/10.1093/rpd/ncr010
9 T. Geber, M. Gunnarsson, and S. Mattsson: Radiat. Meas. **46** (2011) 1248 https://doi.org/10.1016/j.radmeas.2011.07.028
10 U. Häusler, R. Czarwinski, and G. Brix: Eur. Radio. **19** (2009) 2000. https://doi.org/10.1007/s00330-009-1388-4
11 P. J. Gilvin, S. T. Baker, N. J. Gibbens, G. H. Roberts, R. J. Tanner, J. S. Eakins, L. G. Hager, and T. J. Daniels: Radiat. Prot. Dosim. **157** (2013) 430. https://doi.org/10.1093/rpd/nct144
12 P. J. Gilvin, L. Z. Luo, S. T. Baker, C. E. Hill, and J. E. Rotunda: Radiat. Prot. Dosim. **123** (2007) 329. https://doi.org/10.1093/rpd/ncl382
13 H. Hoedlmoser, M. Greiter, V. Bandalo, E. Mende, J. Brönner, P. Kleinau, T. Haninger, M. Furlan, M. Schmid, R. Esser, P. Scheubert, and M. Figel: Radiat. Meas. **125** (2019) 106. https://doi.org/10.1016/j.radmeas.2019.05.002
14 M. Hirakawa, H. Nakatake, S. Tsuruta, S. Matsuura, Y. Motomura, Y. Hiraki, K. Mimori, and K. Ishigami: Interventional Radiol. **7** (2022) 40. https://doi.org/10.22575/interventionalradiology.2022-0005
15 J. Dubeau, J. Sun, N. Leroux, S. Djeffal, and R. Mistry: Radiat. Meas. **167** (2023) 106996. https://doi.org/10.1016/j.radmeas.2023.106996
16 H. Takagi, S. Yanagisawa, Y. Koba, and K. Shinsho: Radiat. Meas. **133** (2020). https://doi.org/10.1016/j.radmeas.2020.106283
17 M. Tanaka, R. Oh, N. Sugioka, H. Tanaka, G. Wakabayashi, S. Sugawara, and K. Shinsho: J. Mater. Sci. - Mater. Electron. **33** (2022) 20271. https://doi.org/10.1007/s10854-022-08843-0
18 K. Shinsho, D. Maruyama, S. Yanagisawa, Y. Koba, M. Kakuta, K. Matsumoto, H. Ushiba, and T. Andoh: Sens. Mater. **30** (2018) 1591.
19 Y. Koba, R. Shimomura, W. Chang, K. Shinsho, S. Yanagisawa, G. Wakabayashi, K.Matsumoto, H. Ushiba, and T. Andoh: Sens. Mater. **30** (2018) 1599. https://doi.org/10.18494/SAM.2018.1930
20 R. Oh, S. Yanagisawa, H. Tanaka, T. Takata, G. Wakabayashi, M. Tanaka, and K. Shinsho: Sens. Mater. **33** (2021) 2129. https://doi.org/10.18494/SAM.2021.3328
21 Physical Measurement Laboratory. Table of contents. NIST: X-Ray Mass Attenuation Coefficients - Copper. https://physics.nist.gov/PhysRefData/XrayMassCoef/ElemTab/z29.html (Accessed Mar 15, 2024).